Chapter 2
Cumulus Cloud Model

Abstract A cumulus cloud model that can explain the observed characteristics of warm rain formation in monsoon clouds is presented. The model is based on classical statistical physical concepts and satisfies the principle of maximum entropy production. Atmospheric flows exhibit self-similar fractal fluctuations that are ubiquitous to all dynamical systems in nature and are characterized by inverse power-law form for power (eddy energy) spectrum signifying long-range space–time correlations. A general systems theory model for atmospheric flows is based on the concept that the large eddy energy is the integrated mean of enclosed turbulent (small-scale) eddies. This model gives scale-free universal governing equations for cloud-growth processes. The model-predicted cloud parameters are in agreement with reported observations, in particular, the cloud drop-size distribution. Rain formation can occur in warm clouds within a 30-min lifetime under favourable conditions of moisture supply in the environment.

Keywords General systems theory · Nonlinear dynamics and chaos · Fractals · Long-range space–time correlations · Inverse power-law eddy energy spectrum · Maximum entropy production principle

2.1 Introduction

The knowledge of the cloud dynamical, microphysical and electrical parameters and their interactions are essential for the understanding of the formation of rain in warm clouds and their modification. Extensive aircraft observations of cloud dynamical, microphysical and electrical parameters have been made in more than 2000 isolated warm cumulus clouds formed during the summer monsoon seasons (June–September) in Pune (18°32′N, 73°51′E, 559 m a.s.l), India (Selvam et al. 1980, 1982a, 1982b, 1982c, 1982d, 1983, 1984a, 1984b, 1984c; Murty et al. 1985; Selvam et al. 1991a, 1991b). The observations were made during aircraft traverses at about 300 m above the cloud base. These observations have provided new evidence relating to the dynamics of monsoon clouds. A brief summary of the important results is given as follows: (i) Horizontal structure of the air flow inside the cloud has consistent variations with successive positive and negative values of vertical velocity representative of ascending and descending air currents inside the

A. M. Selvam, *Rain Formation in Warm Clouds,* SpringerBriefs in Meteorology,
DOI 10.1007/978-3-319-13269-3_2

cloud. (ii) Regions of ascending currents are associated with higher liquid water content (LWC), and negative cloud drop charges and the regions of descending current are associated with lower LWC and positive cloud drop charges. (iii) Width of the ascending and descending currents is about 100 m. The ascending and descending currents are hypothesized to be due to cloud-top-gravity oscillations (Selvam et al. 1982a, 1982b; 1983). The cloud-top-gravity oscillations are generated by the intensification of turbulent eddies due to the buoyant production of energy by the microscale fractional condensation (MFC) in turbulent eddies. (iv) Measured LWC (q) at the cloud-base levels is smaller than the adiabatic value (q_a) with $q/q_a = 0.6$. The LWC increases with height from the base of the cloud and decreases towards the cloud-top regions. (v) Cloud electrical activity is found to increase with the cloud LWC. (vi) Cloud-drop spectra are unimodal near the cloud base and multimodal at higher levels. The variations in mean volume diameter (MVD) are similar to those in the LWC. (vii) In-cloud temperatures are colder than the environment. (viii) The lapse rates of the temperatures inside the cloud are less than the immediate environment. Environmental lapse rates are equal to the saturated adiabatic value. (ix) Increments in the LWC are associated with increments in the temperature inside the cloud. The increments in temperature are associated with the increments in temperature of the immediate environment at the same level or the level immediately above. (x) Variances of in-cloud temperature and humidity are higher in the regions where the values of LWC are higher (Selvam et al. 1982a, 1982b, 1982c, 1982d). The variances of temperature and humidity are larger in the clear-air environment than in the cloud air (Selvam et al. 1982a, 1982b, 1982c, 1982d).

The dynamical and physical characteristics of monsoon clouds described above cannot be explained by simple entraining cloud models. A simple cumulus cloud model, which can explain the observed cloud characteristics, has been developed (Selvam et al. 1983). The relevant physical concept and theory relating to the dynamics of atmospheric planetary boundary layer (PBL), formation of warm cumulus clouds and their modification through hygroscopic particle seeding are presented in the following sections.

The mechanism of large eddy growth, discussed in Sect. 2.4, in the atmospheric ABL can be applied to the formulation of the governing equations for cumulus cloud growth. Based on the above theory, equations are derived for the in-cloud vertical profiles of (i) ratio of actual cloud LWC (q) to the adiabatic LWC (q_a), (ii) vertical velocity, (iii) temperature excess, (iv) temperature lapse rate, (v) total LWC (q_t), (vi) cloud growth time, (vii) cloud drop-size spectrum, and (viii) raindrop size spectrum. The equations are derived starting from the MFC process at cloud-base levels. This provides the basic energy input for the total cloud growth.

2.1.1 Vertical Profile of q/q_a

The observations of cloud LWC, q, indicate that the ratio q/q_a is less than 1 due to dilution by vertical mixing. The fractional volume dilution rate f in the cloud updraft can be computed (Selvam et al. 1983; Selvam et al. 1984a; Selvam et al. 1984b, Selvam 1990, 2007) from Eq. (8) (see Sect. 1.5.3) given by

$$f = \sqrt{\frac{2}{\pi z}} \ln z.$$

In the above equation, f represents the fraction of the air mass of the surface origin which reaches the height z after dilution by vertical mixing caused by the turbulent eddy fluctuations.

Considering that the cloud-base level is 1000 m, the value of $R = 1000$ m and the value of turbulence length scale r below cloud base is equal to 100 m so that the normalized length scale $z = R/r = 1000$ m/100 m $= 10$, and the corresponding fractional volume dilution $f = 0.6$.

The value of q/q_a at the cloud-base level is also found to be about 0.6 by several observers (Warner 1970).

The fractional volume dilution f will also represent the ratio q/q_a inside the cloud. The observed (Warner 1970) q/q_a profile inside the cloud is seen (closely) to follow the profile obtained by the model for dominant eddy radius $r = 1$ m (Fig. 1.4). It is, therefore, inferred that, inside the cloud, the dominant turbulent eddy radius is 1 m, while below the cloud base, the dominant turbulent eddy radius is 100 m.

2.1.2 In-Cloud Vertical Velocity Profile

The logarithmic wind-profile relationship (Eq. 1.4) derived for the PBL in Sect. 1.5.2 holds good for conditions inside a cloud because the same basic physical process, namely MFC, operates in both the cases. The value of vertical velocity inside the cloud will, however, be much higher than in cloud-free air.

From Eq. (1.6), the in-cloud vertical velocity profile can be expressed as

$$W = w_* fz,$$

where W is the vertical velocity at height z, w_* is the production of vertical velocity per second by the MFC at the reference level, i.e. cloud-base level, and f is the fractional upward mass flux of air at level z originating from the cloud-base level.

The f profile is shown in Fig. 1.4. The vertical velocity profile will follow the fz profile assuming w_* is the constant at the cloud-base level during the cloud-growth period.

2.1.3 In-Cloud Excess Temperature Perturbation Profile

The relationship between temperature perturbation θ and the corresponding vertical velocity perturbation is given as follows:

$$W = \frac{g}{\theta_0}\theta,$$

where g is the acceleration due to gravity and θ_0 is the reference-level potential temperature at the cloud-base level.

By substituting for W and taking θ_* as the production of temperature perturbation at the cloud-base level by MFC, we arrive at the following expression since there is a linear relationship between the vertical velocity perturbation W and temperature perturbation θ (from Eqs. 1.4 and 1.6):

$$\theta = \frac{\theta_*}{k} \ln z = \theta_* fz. \tag{2.1}$$

Thus, the in-cloud vertical velocity and temperature perturbation follow the fz distribution (Fig. 1.5).

2.1.4 In-Cloud Temperature Lapse Rate Profile

The saturated adiabatic lapse rate Γ_{sat} is expressed as

$$\Gamma_{\text{sat}} = \Gamma - \frac{L}{C_{\text{p}}} \frac{\mathrm{d}\chi}{\mathrm{d}z},$$

where Γ is the dry adiabatic lapse rate, C_{p} is the specific heat of air at constant pressure, and $\mathrm{d}\chi/\mathrm{d}z$ is the liquid water condensed during parcel ascent along a saturated adiabat Γ_{sat} in a height interval $\mathrm{d}z$.

In the case of cloud growth with vertical mixing, the in-cloud lapse rate Γ_{s} can be written as

$$\Gamma_{\text{s}} = \Gamma - \frac{L}{C_{\text{p}}} \frac{\mathrm{d}q}{\mathrm{d}z},$$

where $\mathrm{d}q$, which is less than $\mathrm{d}\chi$, is the liquid water condensed during a parcel ascent $\mathrm{d}z$ and q is less than the adiabatic LWC q_{a}. From Eq. (2.1),

$$\Gamma_{\text{s}} = \Gamma - \frac{\mathrm{d}\theta}{\mathrm{d}z} = \Gamma - \frac{\theta}{r} = \Gamma - \frac{\theta_* fz}{r}, \tag{2.2}$$

where $\mathrm{d}\theta$ is the temperature perturbation θ during parcel ascent $\mathrm{d}z$. By concept, $\mathrm{d}z$ is the dominant turbulent eddy radius r (Fig. 1.2).

2.1.5 Total Cloud LWC Profile

The total cloud LWC q_{t} at any level is directly proportional to θ as given by the following expression:

$$q_t = \frac{C_p}{L}\theta = \frac{C_p}{L}\theta_* fz = q_* fz, \tag{2.3}$$

where q_* is the production of LWC at the cloud-base level and is equal to $C_p\theta_*/L$. The total cloud LWC q_t profile follows the fz distribution (Fig. 1.5).

2.1.5.1 Cloud-Growth Time

The large eddy-growth time (Eq. 1.36) can be used to compute cloud-growth time T_c:

$$T_c = \frac{r_*}{w_*}\sqrt{\frac{\pi}{2}}\mathrm{li}(\sqrt{z})_{z_1}^{z_2}, \tag{2.4}$$

where li is the Soldner's integral or the logarithm integral. The cloud growth time T_c using Eq. (2.4) is shown in Fig. 2.1.

2.2 Cloud Model Predictions and Comparison with Observations

Numerical computations of cloud parameters were performed for two different cloud-base cloud condensation nuclei (CCN) mean volume radii, namely 2.2 and 2.5 μm, and computed values are compared with the observations. The results are discussed below.

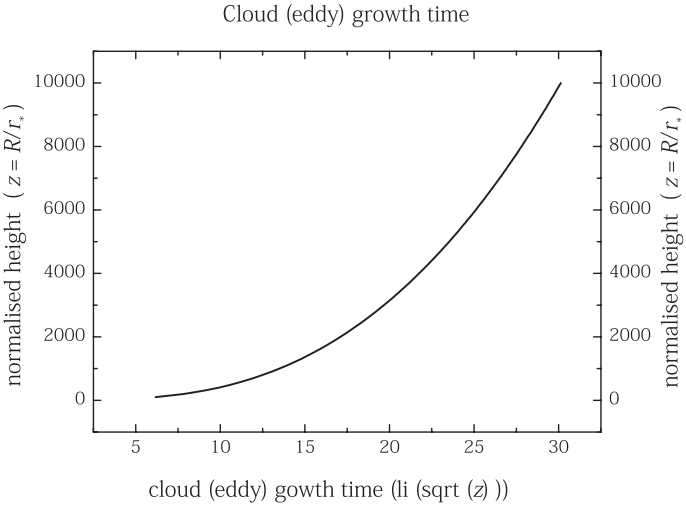

Fig. 2.1 Cloud (large eddy) growth time

2.2.1 Vertical Velocity Profile in the Atmospheric Boundary Layer

The MFC-generated values of vertical velocity have been calculated for different heights above the surface for clear air conditions and above the cloud base for in-cloud conditions for a representative tropical environment with favourable moisture supply. A representative cloud-base height is considered to be 1000 m above sea level (a.s.l), and the corresponding meteorological parameters are surface pressure 1000 mb, surface temperature 30 °C, relative humidity at the surface 80 % and turbulent length scale 1 cm. The values of the latent heat of vaporisation L_V and the specific heat of air at constant pressure C_p are 600 and 0.24 cal gm^{-1}, respectively. The ratio values of m_w/m_0, where m_0 is the mass of the hygroscopic nuclei per unit volume of air and m_w is the mass of water condensed on m_0, at various relative humidities as given by Winkler and Junge (1971, 1972) have been adopted and the value of m_w/m_0 is equal to about 3 for relative humidity of 80 %. For a representative value of m_0 equal to 100 μg m^{-3}, the temperature perturbation θ' is equal to 0.00065 °C, and the corresponding vertical velocity perturbation (turbulent) w_* is computed and is equal to 21.1×10^{-4} cm s^{-1} from the following relationship between the corresponding virtual potential temperature θ_v, and the acceleration due to gravity g, which is equal to 980.6 cm s^{-2}:

$$w_* = \frac{g}{\theta_v}\theta'.$$

Heat generated by the condensation of water equal to 300 μg on 100 μg of hygroscopic nuclei per metre cube, say in 1 s, generates vertical velocity perturbation w_* (cm s^{-2}) equal to 21.1×10^{-4} cm s^{-2} at surface levels. Since the time duration for water vapour condensation by deliquescence is not known, in the following it is shown that a value of w_* equal to 30×10^{-7} cm s^{-2}, i.e. about three orders of magnitude less than that shown in the above example is sufficient to generate clouds as observed in practice.

From the logarithmic wind-profile relationship (Eq. 1.4) and the steady state fractional upward mass flux f of surface air at any height z (Eq. 1.8), the corresponding vertical velocity perturbation W can be expressed in terms of the primary vertical velocity perturbation w_* as (Eq. 1.6):

$$W = w_* f z,$$

W may be expressed in terms of the scale ratio z as follows:

From Eq. (1.8),

$$f = \sqrt{\frac{2}{\pi z}} \ln z.$$

Therefore,

$$W = w_* z \sqrt{\frac{2}{\pi z}} \ln z = w_* \sqrt{\frac{2z}{\pi}} \ln z.$$

Table 2.1 Vertical profile of eddy vertical velocity perturbation W

Height above surface R	Length scale ratio $z=R/r_*$	Vertical velocity $W=w_*fz$ cm s^{-1}
1 cm	1 ($r_*=1$ cm)	$30\times10^{-7}(=w_*)$
100 cm	100	1.10×10^{-4}
100 m	100×100	2.20×10^{-3}
1 km	1000×100	$8.71\times10^{-3}\approx0.01$
10 km	10000×100	3.31×10^{-2}

The values of large eddy vertical velocity perturbation W produced by the process of MFC at normalized height z computed from Eq. 1.6 are given in Table 2.1. The turbulence length scale r_* is equal to 1 cm, and the related vertical velocity perturbation w_* is equal to 30×10^{-7} cm/s for the height interval 1 cm to 1000 m (cloud-base level) for the computations shown in Table 2.1. Progressive growth of successively larger eddies generates a continuous spectrum of semipermanent eddies anchored to the surface and with increasing circulation speed W.

The above values of vertical velocity, although small in magnitude, are present for long enough time period in the lower levels and contribute to the formation and development of clouds as explained in the next section.

2.2.2 Large Eddy-Growth Time

The time T required for the large eddy of radius R to grow from the primary turbulence scale radius r_* is computed from Eq. (1.36) as follows:

$$T=\frac{r_*}{w_*}\sqrt{\frac{\pi}{2}}\int_{x1}^{x2}\mathrm{li}(\sqrt{z}).$$

$$x_1=\sqrt{z_1}\ \text{and}\ x_2=\sqrt{z_2}.$$

In the above equation, z_1 and z_2 refer, respectively, to the lower and upper limits of integration and li is the Soldner's integral or the logarithm integral. The large eddy-growth time T can be computed from Eq. (1.36) as follows.

As explained earlier, a continuous spectrum of eddies with progressively increasing speed (Table 2.1) anchored to the surface grows by MFC originating in turbulent fluctuations at the planetary surface. The eddy of radius 1000 m has a circulation speed equal to 0.01 cm/s (Table 2.1). The time T seconds taken for the evolution of the 1000-m (10^5 cm) eddy from 1 cm height at the surface can be computed from the above equation by substituting for $z_1=1$ cm and $z_2=10^5$ cm such that $x_1=1$ and $x_2\approx317$.

$$T=\frac{1}{0.01}\sqrt{\frac{\pi}{2}}\int_{1}^{317}\mathrm{li}(z).$$

The value of $\int_1^{317} \mathrm{li}(z)$ is equal to 71.3.

Hence, $T \approx 8938$, s ≈ 2 h 30 min.

Thus, starting from the surface level cloud growth begins after 2 h 30 min. This is consistent with the observations that under favourable synoptic conditions solar surface heating during the afternoon hours gives rise to cloud formation.

The dominant turbulent eddy radius at 1000 m in the sub-cloud layer is 100 m starting from the 1-cm-radius dominant turbulent eddy at surface and the formation of successively larger dominant eddies at decadic length scale intervals as explained in Sect. 1.5.1. Also, it has been shown in Sect. 2.1.1 that the radius of the dominant turbulent eddy (r_*) inside the cloud is 1 m. These features suggest that the scale ratio is 100 times larger inside the cloud than below the cloud. The 1000-m (1 km) eddy at cloud-base level forms the internal circulation for the next stage of eddy growth, namely 10 km eddy radius with circulation speed equal to 0.03 cm/s. Cloud growth begins at 1 km above the surface and inside this 10-km eddy, with dominant turbulent eddy radius 1 m as shown above. The circulation speed of this 1-m-radius eddy inside cloud is equal to 3 m/s as shown in the following. Since the eddy continuum ranging from 1 cm to 10 km radius grows from the surface starting from the same primary eddy of radius r_* and the perturbation speed w_* (cm/s), the circulation speeds of any two eddies of radii R_1, R_2 with corresponding circulation speeds W_1 and W_2 are related to each other as follows from Eq. (1.1):

$$W_1^2 = \sqrt{\frac{2}{\pi}} \frac{r_*}{R_1} w_*^2,$$

$$W_2^2 = \sqrt{\frac{2}{\pi}} \frac{r_*}{R_2} w_*^2,$$

$$\frac{W_2^2}{W_1^2} = \frac{R_1}{R_2},$$

$$\frac{W_2}{W_1} = \sqrt{\frac{R_1}{R_2}}.$$

As mentioned earlier, cloud growth with dominant turbulent eddy radius 1 m begins at 1 km above surface and forms the internal circulation to the 10-km eddy. The circulation speed of the in-cloud dominant turbulent eddy is computed as equal to 3 m/s from the above equation where the subscripts 1 and 2 refer, respectively, to the outer 10-km eddy and the internal 1-m eddy.

The value of vertical velocity perturbation W at cloud base is then equal to 100 times the vertical velocity perturbation just below the cloud base. Vertical velocity perturbation just below the cloud base is equal to 0.03 cm/s from Table 2.1. Therefore, the vertical velocity perturbation at cloud base is equal to 0.03 × 100 cm/s, i.e. 3 cm/s and is consistent with airborne observations over the Indian region during the monsoon season (Selvam et al. 1976; Pandithurai et al. 2011).

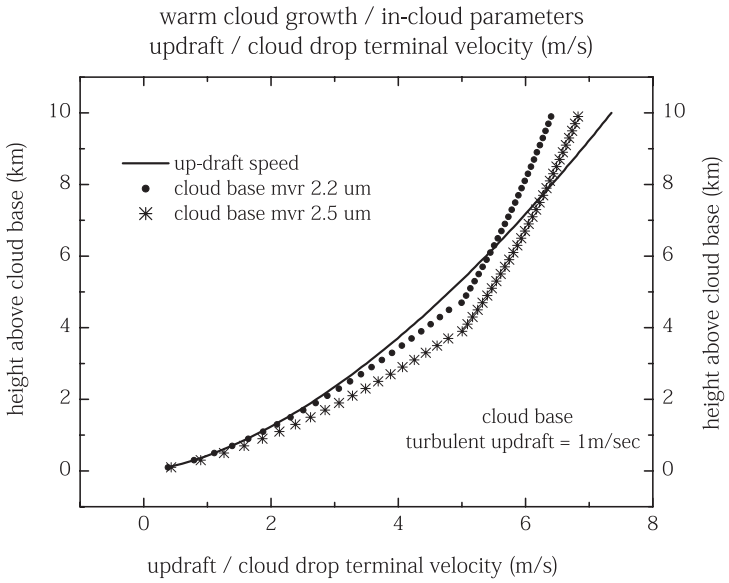

Fig. 2.2 In-cloud updraft speed and cloud particle terminal velocities for the two input cloud-base CCN size spectra with mean volume radius (mvr) equal to (i) 2.2 μm and (ii) 2.5 μm. CCN cloud condensation nuclei

Cloud-base vertical velocity equal to 1 cm/s has been used for the model computations in the following. The in-cloud updraft speed and cloud particle terminal velocities are given in Fig. 2.2 for the two input cloud-base CCN size spectra with mean volume radius (mvr) equal to (i) 2.2 μm and (ii) 2.5 μm. The in-cloud updraft speed W is the same for both CCN spectra since $W = w_* fz$ (Eq. 1.6) and depends only on the persistent cloud-base primary perturbation speed w_* originating from MFC by deliquescence on hygroscopic nuclei at surface levels in humid environment (see Sect. 1.3). Cloud LWC increases with height (Fig. 2.3) associated with the increase in cloud particle mean volume radius (Fig. 2.4) and terminal velocities (Fig. 2.2). The cloud particles originating from the larger size CCN (mvr = 2.5 μm) are associated with larger cloud LWCs, larger mean volume radii, and, therefore, larger terminal fall speeds at all levels.

The turbulent vertical velocity perturbation w_* at cloud-base level (1 km) is equal to 0.01 m/s or 1 cm/s. The corresponding cloud-base temperature perturbation θ_* is then computed from the equation:

$$w_* = \frac{g}{\theta_v}\theta_*$$

$$\theta_* = w_* \frac{\theta_v}{g}.$$

Substituting $w_* = 1$ cm/s, $\theta_v = 273 + 30 = 303$ K and $g = 980.6$ cm/s^2, the temperature perturbation is equal to 0.309 °C and for the 1-m eddy radius the average in-cloud

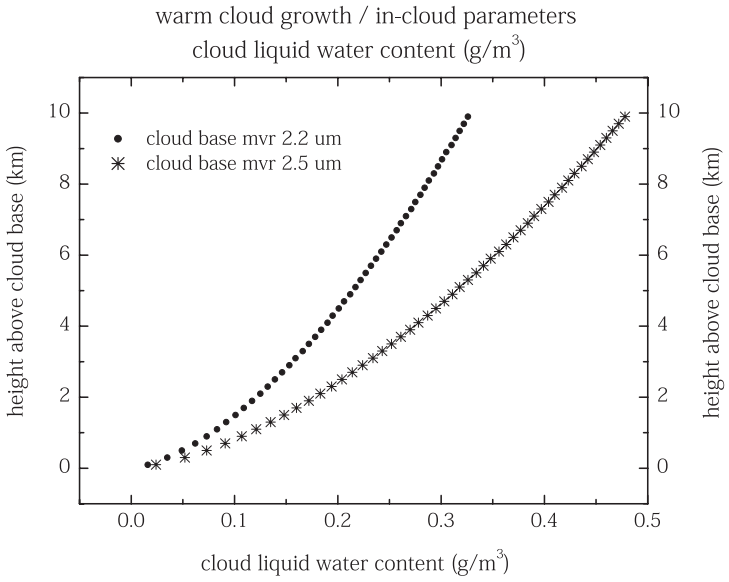

Fig. 2.3 Cloud liquid water content

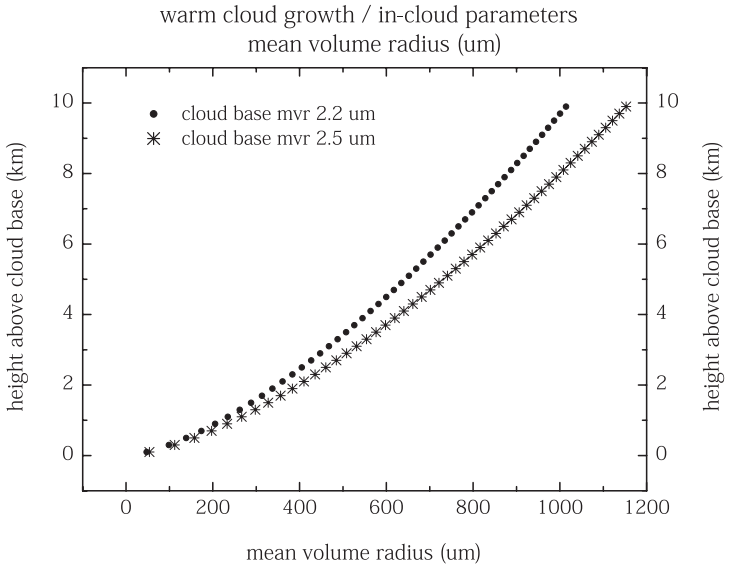

Fig. 2.4 Cloud particle mean volume radius (μm)

temperature perturbation per centimetre is equal to 0.309/100 = 0.00309 °C. The temperature perturbation (warming) $\theta = \theta_* fz$ (Eq. 1.6) increases with height with corresponding decrease in the in-cloud temperature lapse.

2.2.3 In-Cloud Temperature Lapse Rate

The in-cloud lapse rate Γ_s is computed using the following expression (Eq. 2.2):

$$\Gamma_s = \Gamma - \frac{\theta_* fz}{r_*}.$$

The primary eddy radius length r_* at cloud base is equal to 1 m as shown earlier (Sect. 2.1). The model computations for in-cloud vertical profile of vertical velocity W, temperature perturbation θ and lapse rate Γ_c at 1 km height intervals above the cloud base are given in Table 2.2.

The predicted temperature lapse rate decreases with height and becomes less saturated than adiabatic lapse rate near the cloud top, the in-cloud temperatures being warmer than the environment. These results are in agreement with the observations.

2.2.4 Cloud-Growth Time

The large eddy-growth time (Eq. 1.36) can be used to compute cloud-growth time T_c (Eq. 2.4):

$$T_c = \frac{r_*}{w_*}\sqrt{\frac{\pi}{2}}\mathrm{li}(\sqrt{z})_{z_1}^{z_2},$$

where li is the Soldner's integral or the logarithm integral. The vertical profile of cloud-growth time T_c is a function of the cloud-base primary turbulent eddy fluctuations of radius r_* and perturbation speed w_* alone. The cloud-growth time T_c using Eq. (2.4) is shown in Fig. 2.5 for the two different cloud-base CCN spectra, with mean volume radii equal to 2.2 and 2.5 μm, respectively. The cloud-growth time remains the same since the primary trigger for cloud growth is the persistent turbulent energy generation by condensation at the cloud base in primary turbulent eddy fluctuations of radius r_* and perturbation speed w_*.

Let us consider r_* is equal to 100 cm and w_* is equal to 1 cm s^{-1} the time taken for the cloud to grow (see Sect. 2.1.6) to a height of, e.g. 1600 m above cloud base can be computed as shown below. The normalized height z is equal to 1600 since dominant turbulent eddy radius is equal to 1 m:

$$\begin{aligned} T_c &= \frac{100}{100\times 0.01}\sqrt{\frac{\pi}{2}}\mathrm{li}\sqrt{1600} \\ &= 100\times 1.2536\times 15.84\ s \\ &\approx 30\ \text{min}. \end{aligned}$$

The above value is consistent with cloud-growth time observed in practice.

Table 2.2 In-cloud vertical velocity and temperature lapse rates

Sl. No.	Height above cloud base R(m)	Scale ratio $z=R/r_*$, ($r_*=1$ m)	f	fz	In-cloud vertical velocity (ms^{-1}) $W=w_*fz$ms^{-1}, $w_*=.01$ ms^{-1}	In-cloud temperature perturbation C $\theta=(\theta_* fz)$ C $\theta_*=0.00309$C	In-cloud lapse rate Γ_cC/km $\Gamma_c=\Gamma-\theta$ $\Gamma=-10$ C/km
1	1000	1000	0.17426	174.26	1.74	0.538	−9.46
2	2000	2000	0.13558	271.16	2.71	0.838	−9.16
3	3000	3000	0.11661	349.82	3.50	1.081	−8.92
4	4000	4000	0.10461	418.46	4.18	1.293	−8.70
5	5000	5000	0.09609	480.43	4.80	1.484	−8.52
6	6000	6000	0.08959	537.56	5.38	1.661	−8.34
7	7000	7000	0.08442	590.91	5.91	1.826	−8.17
8	8000	8000	0.08016	641.24	6.41	1.981	−8.01
9	9000	9000	0.07656	689.05	6.89	2.129	−7.87
10	10,000	10,000	0.07347	734.73	7.34	2.270	−7.72

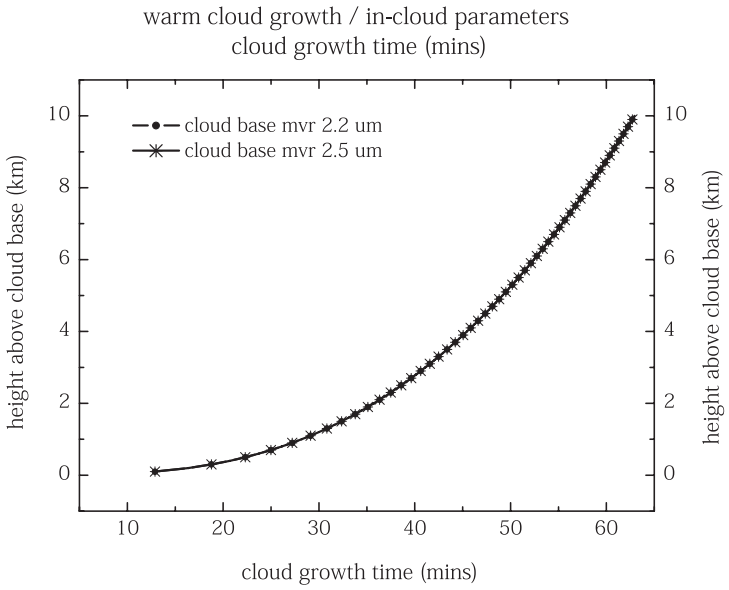

Fig. 2.5 Cloud-growth time

2.2.5 Cloud Drop-Size Spectrum

The evolution of cloud drop-size spectrum is critically dependent on the water vapour available for condensation and the nuclei number concentration in the sub-cloud layer. Cloud drops form as water vapour condenses in the air parcel ascending from cloud-base levels. Vertical mixing during ascent reduces the volume of cloud-base air reaching higher levels to a fraction *f* of its initial volume. Thus, the nuclei available for condensation, i.e. the cloud drops number concentration also decreases with height according to the *f* distribution. The total cloud-water content was earlier shown (Eq. 1.6) to increase with height according to the *fz* distribution. Thus, bigger size cloud drops are formed on the lesser number of condensation nuclei available at higher levels in the cloud. Due to vertical mixing, unsaturated conditions exist inside the cloud. Water vapour condenses on fresh nuclei available at each level, since, in the unsaturated in-cloud conditions, MFC occurs preferentially on small condensation nuclei (Pruppacher and Klett 1997).

Earlier in Sect. 1.6, it was shown that the atmospheric eddy continuum fluctuations hold in suspension atmospheric particulates, namely aerosols, cloud droplets and raindrops. The cloud drop-size distribution spectrum also follows the universal spectrum derived earlier for atmospheric aerosol size distribution.

2.2.6 In-Cloud Raindrop Spectra

In the cloud model, it is assumed that bulk conversion of cloud water to rainwater takes place mainly by collection, and the process is efficient due to the rapid increase in the cloud-water flux with height. The in-cloud raindrop size distribution also follows the universal spectrum derived earlier for the suspended particulates in the atmosphere (Sect. 1.6.4).

The total rainwater content Q_r (c.c) is given as

$$Q_r = \frac{4}{3}\pi r_a^3 N = \frac{4}{3}\pi r_{as}^3 N_* f z^2 \cdot \tag{2.5}$$

The above concept of raindrop formation is not dependent on the individual drop collision coalescence process.

Due to the rapid increase of cloud water flux with height, bulk conversion to rain water takes place in time intervals much shorter than the time required for the conventional collision–coalescence process.

The cloud-base CCN size spectrum and the in-cloud particle (cloud and raindrop) size spectrum follow the universal spectrum (Fig. 1.8) for suspended particulates in turbulent fluid flows. The cloud-base CCN spectra and the in-cloud particulates (cloud and raindrops) size spectra at two levels, 100 m and 2 km, plotted in conventional manner as dN/Nd (log R) versus R on log–log scale are shown in Fig. 2.6. The in-cloud particulate size spectrum shifts rapidly towards larger sizes associated with

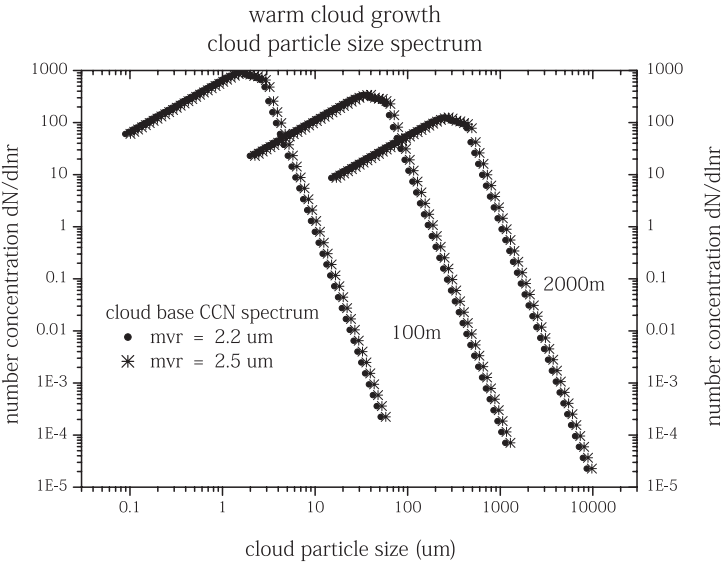

Fig. 2.6 Cloud-base CCN spectra and the in-cloud particulates (cloud and raindrops) size spectra at two levels—100 m and 2 km. CCN cloud condensation nuclei

rain formation. According to the general systems theory for suspended particulate size spectrum in turbulent fluid flows (Sect. 1.6), larger suspended particulates are associated with the turbulent regions (smaller scale length with larger fluctuation speed) of the vertical velocity spectrum. Spontaneous formation of larger cloud/raindrops may occur by collision and coalescence of smaller drops in these regions of enhanced turbulence.

2.2.7 Rainfall Commencement

Rainfall sets in at the height at which the terminal velocity w_T of the raindrop becomes equal to the mean cloud updraft W. Let the mean volume radius R_m be representative of the precipitation drop at level z above cloud base. In the intermediate range (40 μm $< R_m <$ 0.6 mm), an approximated formula for the fall speed is given by Yau and Rogers (1989) as $w_T = K_3 R_m$, where $K_3 = 8 \times 10^3$ s^{-1}.

For droplets with radii $<$30 μm, the terminal velocity is given as $w_T = K_1 R_m^2$, where $K_1 \sim 1.19 \times 10^6$ cm^{-1} s^{-1}.

For large drops, $w_T = K_2 \sqrt{R_m}$. K_2 can be approximated as $K_2 = 2010$ cm$^{1/2}$ s^{-1} for a raindrop size between 0.6 and 2 mm (Yau and Rogers 1989).

2.2.8 Rainfall Rate

The in-cloud rainfall rate (R_t) can be computed as shown below.

Rain water production rate over unit area (rainfall rate mm/s/unit area) Q_{rt} in the cloud at any level z above the cloud base (Eq. 2.5) is given by

$$R_{tz} = (W_T - W)\frac{4}{3}\pi R_m^3 N.$$

The in-cloud rainfall rate R_{tz} is derived from the normalized flux value for height z, i.e. eddy wavelength z. Therefore, for unit-normalized height interval z, the rainfall rate R_t is equal to R_{tz}/z cm/s.

$$R_t = (R_{tz}/z) \times 3600 \times 10\,\text{mm/h}.$$

In the above equation, W_T in cm/s is the terminal velocity of the raindrop of mean volume radius R_m at level z. Rainfall rate (R_t) derived above is representative of the mean cloud scale rain intensity.

Rain formation computed for two different cloud-base CCN mean volume radius, namely 2.2 and 2.5 μm are shown in Fig. 2.7. Rain with larger rain rate forms at a lower level and extends up to a higher level for the larger size (mean volume radius 2.5 μm) cloud-base CCN spectrum.

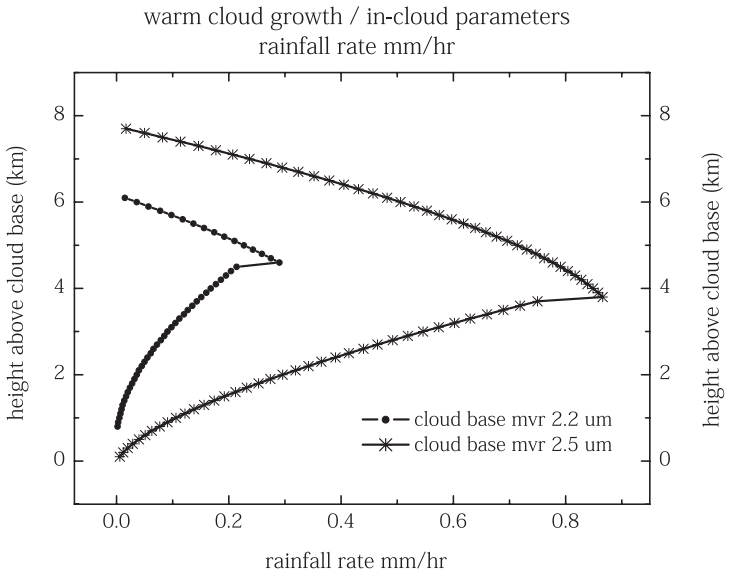

Fig. 2.7 In-cloud rain rate (mm/h)

2.3 Warm Cloud Responses to Hygroscopic Particle Seeding

In Sects. 1.3 and 1.4, it is shown that the production of buoyant energy released by condensation in turbulent eddies is mainly responsible for the formation and growth of the cloud. When warm clouds are seeded with hygroscopic particles, the turbulent buoyant energy production increases due to condensation and results in enhancement of vertical mass exchange. This would result in enhancement of convergence in the sub-cloud layer and invigoration of the updraft in the cloud. If sufficient moisture is available in the sub-cloud air layer, the enhanced convergence would lead to increased condensation and cloud growth. According to the above physical concept and theory of the cumulus cloud model presented in this chapter, it can be concluded that hygroscopic particle seeding alters the dynamics of warm clouds.

2.3.1 Dynamic Effect of Salt Seeding

Woodcock and Spencer (1967) hypothesized that dispersion of NaCl particles in a nearly water-saturated atmosphere would be sufficient to initiate a cumulus cloud. Their experiments have produced visible clouds when dry NaCl particles in the size range 0.5–20 μm diameter, were released from the aircraft in the warm moist marine boundary layer near Hawaii. The temperatures in the salt-laden air were about 0.4 °C higher than that of the environment on the average. Observations of

the possible dynamic effects in warm clouds by hygroscopic particle seeding have been recorded (Murty et al. 1975, 1981; Parasnis et al. 1982). The dynamic effect of salt seeding has been estimated from the following calculations that are based on the theory and the physical concept of the cumulus cloud model discussed earlier.

The latent heat released by condensation on the hygroscopic nuclei is computed for the turbulent vertical velocities of 1 m/s and the turbulent eddy radius of 50 m. The relative humidity inside the cloud at the seeding level near the cloud base is assumed to be equal to 90 %. A seeding rate of 500 g/s and a volume dispersion rate of 45,000 m^3/s are assumed. The value of the seeding rate assumed is based on that used in the aircraft warm cloud modification experiment in India (Krishna et al. 1974; Murty et al. 1975). The value of the dispersion rate used in the computation is equal to half the value assumed by Woodcock and Spencer (1967). The median volume diameter of the salt nuclei is 10 μm. One such nucleus gives rise to the formation of a water droplet of radius 9.5 μm in a time period of 1 s at the assumed relative humidity of 90 % inside the cloud (Keith and Aarons 1954). Thus, the mass of water condensed on the seed nuclei per second per cubic metre of the seeded volume can be computed. The latent heat released by this condensation will give rise to a heating rate of 0.09 cm^{-3} s^{-1} of the seeded volume. The temperature increase will result in a vertical velocity increase of about 0.3 cm s^{-2}. This increase in the vertical velocity occurs in successive 50 m lengths of the cloud along the flight path of the aircraft whose speed is 50 m s^{-1}. The mean increase in the turbulent vertical velocity along a 500 m length of the cloud can be approximately taken to be equal to one tenth of the vertical velocity in individual 50 m length of aircraft path, i.e. equal to 0.03 cm s^{-2}. Therefore, the mean increase in the vertical velocity for the total path length of 500 m, i.e. the large eddy updraft region is equal to one fourth of the mean increase in turbulent vertical velocity (Eq. 1.1). Thus, the vertical velocity perturbation in large eddy updraft region is equal to about 0.01 cm s^{-2}. This cloud scale vertical velocity perturbation due to the hygroscopic particle seeding is equal to the naturally occurring vertical velocity perturbation at the cloud-base level for the sample cloud case discussed in Sect. 2.2. Also, it was shown that the cloud-base vertical velocity production is the main driving agent for the cloud growth processes. The sample computations of the dynamic effect of salt seeding discussed above indicated that the total cloud-growth processes in the case of seeded clouds would be increased by 100 %. Evidence of such dynamic effects due to salt seeding in warm cumulus clouds (Fig. 2.8) can be seen from the observation of cloud LWC, in-cloud temperature and cloud-top growth rates made in seeded clouds (Murty et al. 1975; Murty et al. 1981, Murty et al., 2000).

Conclusions

Atmospheric flows exhibit self-similar fractal fluctuations, a signature of long-range correlations on all space–time scales. Realistic simulation and prediction of atmospheric flows require the incorporation of the physics of observed fractal

Fig. 2.8 Seeded cloud that developed rain following seeding in 20 min. Fall streak of the raining cloud is clearly seen in the photograph (Murty et al. 2000)

fluctuation characteristics in traditional meteorological theory. A general systems theory model for fractal space–time fluctuations in turbulent atmospheric flows (Selvam 1990, 2007, 2009, 2012a, b, 2013, 2014) is presented. Classical statistical physical concepts underlie the physical hypothesis relating to the dynamics of the atmospheric eddy systems and satisfy the maximum entropy principle of statistical physics. The model predictions are as follows:

- Fractal fluctuations of atmospheric flows signify an underlying eddy continuum with overall logarithmic spiral trajectory enclosing a nested continuum of vortex-roll circulations that trace the quasi-periodic Penrose-tiling pattern. Satellite images of cyclones and hurricanes show the vivid logarithmic spiral cloud pattern whose precise mathematical equiangular spiral (golden) geometry has been used by meteorologists (Senn et al. 1957; Senn and Hisar 1959; Sivaramakrishnan and Selvam 1966; Wong et al. 2008) for locating the centre (eye) of the storm.
- The logarithmic law of wall for boundary layer flows is derived as a natural consequence of eddy mixing process. The von Karman's constant is equal to $1/\tau^2$ (≈ 0.38), where τ is the golden mean (≈ 0.618).

- The probability distribution for amplitude as well as variance of fractal fluctuations of meteorological parameters are given by the same universal inverse power-law function *P,* namely $P=\tau^{-4t}$ where the normalized standard deviation *t* designates the eddy length step growth number. Such a result that the additive amplitudes of eddies when squared represent the probability densities of the fluctuations is observed in the subatomic dynamics of quantum systems. Therefore, fractal fluctuations are signatures of quantum-like chaos in dynamical systems.
- The probability distribution *P* of amplitudes of fractal fluctuations is close to the statistical normal distribution for values of normalized standard deviation *t* values equal to or less than two. The probability of occurrence of extreme events, i.e. normalized deviation *t* values greater than two, is close to zero as given by the statistical normal distribution, while *P* distribution for fractal fluctuations gives appreciably high values as observed in practice.
- Atmospheric eddy energy (variance) spectrum follows the universal inverse power-law form $P=\tau^{-4t}$ indicating long-range space–time correlations between local (small-scale) and global (large-scale) perturbations.
- Atmospheric particulates are suspended in the fractal fluctuations of vertical velocities with amplitudes given by the universal inverse power-law *P*. A universal scale-independent mass or radius size distribution for homogeneous suspended atmospheric particulates is expressed as a function of the golden mean τ, the total number concentration and the mean volume radius. The general systems theory model for aerosol size distribution is scale-free and is derived directly from atmospheric eddy dynamical concepts. At present, empirical models such as the log-normal distribution with arbitrary constants for the size distribution of atmospheric suspended particulates are used for quantitative estimation of earth-atmosphere radiation budget related to climate warming/cooling trends.
- Numerical computations of cloud parameters were performed for two different cloud-base CCN mean volume radius, namely 2.2 and 2.5 μm and computed values are compared with the observations. Cloud-base vertical velocity production by MFC is the main driving agent for the cloud growth processes. The cloud-growth time is about 30 min as observed in practice (McGraw and Liu 2003) and is the same for the two CCN spectra since the primary trigger for cloud growth is the persistent turbulent energy generation by condensation at the cloud base in primary turbulent eddy fluctuations of radius r_* and perturbation speed w_*. However, for the larger CCN mean volume radius, namely 2.5 μm, raindrops form earlier at a lower level and extend up to higher levels in the cloud. Under suitable conditions of humidity and moisture in the environment, warm rain formation can occur at a time interval short as 30 min.
- Hygroscopic particle seeding alters the dynamics of warm clouds and enhances rainfall up to 100 % under favourable conditions of moisture supply in the environment.

References

Keith CH, Arons AB (1954) The growth of sea-salt particles by condensation of atmospheric water vapour. J Meteor 11:173–184

Krishna K, Murty ASR, Kapoor RK, Ramanamurty BhV (1974) Results of warm cloud seeding experiments in three different regions in India during the summer monsoon of 1973. Proc. IV Conf. Wea. Modification 18-21 November 1974, Fort Lauderdale, Florida, Amer. Meteor. Soc. 79–84

McGraw R, Liu Y (2003) Kinetic potential and barrier crossing: a model for warm cloud drizzle formation. Phys Rev Lett 90(1):018501–018501

Murty ASR, Selvam AM, Ramanamurty BhV (1975) Summary of observations indicating dynamic effect of salt seeding in warm cumulus clouds. J Appl Meteor 14:629–637

Murty ASR, Selvam AM, Bandyopadhyay BK, Revathy N, Pillai AG, Ramanamurty BhV (1981) Electrical and microphysical responses to salt seeding in maritime cumulus clouds. J Wea Modification 13:174–176

Murty ASR, Selvam AM, Devara PCS, Krishna K, Chatterjee RN, Mukherjee BK, Khemani LT, Momin GA, Reddy RS, Sharma SK, Jadhav DB, Vijayakumar R, Raj PE, Manohar GK, Kandalgaonkar SS, Paul SK, Pillai AG, Parasnis SS, Kulkarni CP, Londhe AL, Bhosale CS, Morwal SB, Safai PD, Pathan JM, Indira K, Naik MS, Rao PSP, Sikka P, Dani KK, Kulkarni MK, Trimbake HK, Sharma PN, Kapoor RK, Tinmaker MIR (2000) 11-year warm cloud modification experiment in Maharashtra State, India. J Wea Modification 32:10–20

Pandithurai G, Dipu S, Prabha TV, Maheskumar RS, Kulkarni JR, Goswami BN (2012) Aerosol effect on droplet spectral dispersion in warm continental cumuli. J Geophys Res 117:D16202

Parasnis SS, Selvam AM, Murty ASR, Ramanamurty BhV (1982) Dynamic responses of warm monsoon clouds to salt seeding. J Wea Modification 14:35–37

Pruppacher HR, Klett JD (1997) Microphysics of clouds and precipitation. Kluwer Academic, The Netherlands

Selvam AM, Murty ASR, Vijayakumar R, Ramanamurty BhV (1976) Aircraft measurement of electrical parameters inside monsoon clouds. Indian J Meteor Hydrol Geophys 27:391–396

Selvam AM, Murty ASR, Vijayakumar R, Paul SK, Manohar GK, Reddy RS, Mukherjee BK, Ramanamurty BhV (1980) Some thermodynamical and microphysical aspects of monsoon clouds. Proc Indian Acad Sci 89A:215–230

Selvam AM, Murty ASR, Ramanamurty BhV (1982a) Dynamics of the summer monsoon warm clouds. Proc. Reg. Sci. Conf. Trop. Meteor., 18–22 Oct. 1982, Tsukaba, Japan, 247–248

Selvam AM, Parasnis SS, Murty ASR, Ramanamurty BhV (1982b) Evidence for cloud-top entrainment in the summer monsoon warm cumulus clouds. Proc. Conf. Cloud Phys. 15–18 Nov. 1982, Chicago, Illinois, Amer. Meteor. Soc. 151–154

Selvam AM, Sikka P, Vernekar KG, Manohar GK, Mohan B, Kandalgaonkar SS, Murty ASR, Ramanamurty BhV (1982c) Temperature and humidity spectra in cloud and cloud-free air and associated cloud electrical and microphysical characteristics. Proc. Conf. Cloud Phys. 15–18 Nov. 1982, Chicago, Illinois, Amer. Meteor. Soc. 32–35

Selvam AM, Londhe AL, Vernekar KG, Mohan B, Murty ASR, Ramanamurty BhV (1982d) Aircraft observations of turbulent fluxes of momentum, heat and moisture in the sub-cloud layer and associated cloud microphysical and electrical characteristics. Proc. Conf. Cloud Phys. 15–18 Nov. 1982, Chicago, Illinois, Amer. Meteor. Soc. 42–44

Selvam AM, Murty ASR, Ramanamurty BhV (1983) Surface frictional turbulence as an agent for the maintenance and growth of large eddies in the atmospheric planetary boundary layer. Proc. VI Symp. Turbul. & Diffus., 22–25 March 1983, Boston, Mass., Amer. Meteor. Soc., 106–109

Selvam AM, Murty ASR, Ramanamurty BhV (1984a) A new hypothesis for vertical mixing in clouds. Preprint volume, 9th Intl. Cloud Phys. Conf. Tallinn, USSR

Selvam AM, Murty ASR, Ramanamurty BhV (1984b) Role of frictional turbulence in the evolution of cloud systems. Preprint volume, 9th Intl. Cloud Phys. Conf., Tallinn, USSR

Selvam AM (1990) Deterministic chaos, fractals and quantumlike mechanics in atmospheric flows. Can J Phys 68, 831–841 (http://xxx.lanl.gov/html/physics/0010046)
Selvam AM, Vijayakumar R, Murty ASR (1991a) Some physical aspects of summer monsoon clouds- comparison of cloud model results with observations. Adv Atmos Sci 8(1):111–124
Selvam AM, Vijayakumar R, Manohar GK, Murty ASR (1991b) Electrical, microphysical and dynamical observations in summer monsoon clouds. Atmos Res 26:19–32
Selvam AM (2007) Chaotic climate dynamics. Luniver, UK
Selvam AM (2009) Fractal fluctuations and statistical normal distribution. Fractals 17(3), 333–349 (http://arxiv.org/pdf/0805.3426)
Selvam AM (2012a) Universal spectrum for atmospheric suspended particulates: comparison with observations. Chaos Complex Lett 6(3), 1–43 (http://arxiv.org/abs/1005.1336)
Selvam AM (2012b) Universal spectrum for atmospheric aerosol size distribution: comparison with PCASP-B observations of vocals 2008. Nonlinear Dyn Syst Theory 12(4), 397–434 (http://arxiv.org/abs/1105.0172)
Selvam AM (2013) Scale-free Universal Spectrum for Atmospheric Aerosol Size Distribution for Davos, Mauna Loa and Izana. Int J Bifurcation Chaos 23:1350028
Selvam AM (2014) A general systems theory for rain formation in warm clouds. Chaos Complex Lett 8(1), 1–42 (http://arxiv.org/pdf/arxiv1211.0959)
Senn HV, Hiser HW, Bourret RC (1957) Studies of hurricane spiral bands as observed on radar. Final Report, U. S. Weather Bureau Contract No. Cwb-9066, University of Miami, 21pp. [NTIS-PB-168367]
Senn HV, Hiser HW (1959) On the origin of hurricane spiral bands. J Meteor 16:419–426
Sivaramakrishnan MV, Selvam MM (1966) On the use of the spiral overlay technique for estimating the center positions of tropical cyclones from satellite photographs taken over the Indian region. Proc. 12th conf. Radar Meteor., 440-446
Warner J (1970) The micro structure of cumulus clouds Part III: the nature of updraft. J Atmos Sci 27:682–688
Winkler P, Junge CE (1971) Comments on “Anomalous deliquescence of sea spray aerosols”. J Appl Meteor 10:159–163
Winkler P, Junge C (1972) The growth of atmospheric aerosol particles as a function of the relative humidity. J de Recherches Atmospheriques 6:617–637
Wong KY, Yip CL, Li PW (2008) Automatic identification of weather systems from numerical weather prediction data using genetic algorithm. Expert Syst Appl 35(1–2):542–555
Woodcock AH, Spencer AT (1967) Latent heat released experimentally by adding Sodium Chloride particles to the atmosphere. J Appl Meteor 6:95–101

http://www.springer.com/978-3-319-13268-6

Rain Formation in Warm Clouds
General Systems Theory
Selvam, A.M.
2015, XV, 98 p. 32 illus., 1 illus. in color., Softcover
ISBN: 978-3-319-13268-6